ACS Catalysis

Research Article

Cite This: ACS Catal. 2018, 8, 7270−7278

pubs.acs.org/acscatalysis

Revealing the Size Effect of Platinum Cocatalyst for Photocatalytic Hydrogen Evolution on TiO_2 Support: A DFT Study

Dong Wang,[†,‡] Zhi-Pan Liu,*[,‡] and Wei-Min Yang*[,†]

[†]State Key Laboratory of Green Chemical Engineering and Industrial Catalysis, SINOPEC Shanghai Research Institute of Petrochemical Technology, Shanghai 201208, China

[‡]Collaborative Innovation Center of Chemistry for Energy Material, Shanghai Key Laboratory of Molecular Catalysis and Innovative Materials, Key Laboratory of Computational Physical Science (Ministry of Education), Department of Chemistry, Fudan University, Shanghai 200433, China

Supporting Information

ABSTRACT: In heterogeneous catalysis metal particle morphology and size can influence markedly the activity, both in heat-driven and in electro-photocatalytic conditions. Because of the intimate coupling between the photoelectron transfer and the surface catalytic reaction, it has been challenging to determine the optimal metal particle size in photocatalytic reactions. Here, we utilize ab initio molecular dynamics and hybrid density functional theory calculations to reveal the size-dependent activity of photocatalytic hydrogen evolution reaction (HER) over Pt/TiO_2 photocatalysts. By supporting four different Pt particles Pt_5, Pt_8, Pt_{13}, and Pt_{19} on anatase $TiO_2(101)$, we determine the optimal geometries, the electronic structures, the photoelectron-transfer efficiency, and the surface hydrogen coupling reaction activity of these composite materials. We demonstrate that very small Pt clusters with less than two atomic layers are efficient photoelectron collectors from TiO_2 bulk due to their low highest occupied molecular orbital level with respect to the oxide conduction band; by contrast, larger particles with more than two Pt layers are the active site for hydrogen coupling to catalyze HER. Our results suggest that quasi two-Pt-layer particles, corresponding to ∼1 nm size, are the best catalyst for photocatalytic HER. Compared to heat-driven and electrocatalysis, we conclude that photocatalysis prefers even smaller metal particles to enhance photoelectron transfer, which should be a general guideline for designing optimal photocatalysts in the future.

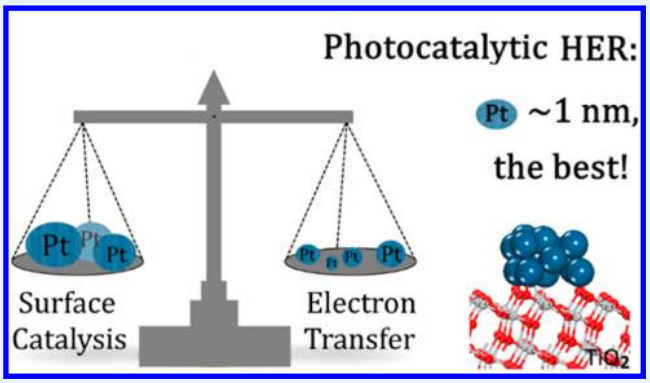

KEYWORDS: *hydrogen evolution, platinum, TiO_2, size effect, photocatalysis, electron transfer, density functional theory*

1. INTRODUCTION

Titanium dioxide (TiO_2) with supported metal cocatalyst receives considerable attention in the past decades for its activity toward water splitting under photocatalytic conditions.[1−3] The presence of metal cocatalysts plays critical roles in promoting the reductive half-reaction, namely, the photocatalytic hydrogen evolution reaction (HER, $2H^+ + 2e^- \rightarrow H_2$). Platinum (Pt) is by far the best metal cocatalyst, which was attributed to the proper Fermi level for accepting photoelectrons and the intrinsic low overpotential for hydrogen production.[4,5] The underlying mechanism for the photocatalytic HER on metal cocatalysts is, however, largely elusive considering that the photocatalytic reaction, unlike heat-driven reactions, involves both the photoelectron transfer from oxide to metal and the catalytic H_2 production on metal. This has led to the great uncertainty on the optimum morphology and size for supported metal particles, the knowledge of which is essential to reduce the usage of Pt and increase the activity.

Recent experiments have revealed strong evidence that the Pt particle size is important to the catalytic activity. Jaroniec et al. reported that metallic Pt supported on TiO_2 nanosheet with average diameter of 2−4 nm prepared using impregnation method, as characterized by high-resolution X-ray photoelectron spectroscopy (XPS), exhibits the highest photocatalytic HER activity; the corresponding H_2 production rate is ∼1.4 times higher than subnano Pt particles with a diameter of 0.5 nm (333.5 vs 236.6 $\mu mol \cdot h^{-1}$), and is comparable with that of ∼1 nm Pt nanoparticles (306.5 $umol \cdot h^{-1}$).[6] With laser ablation and soft-landing methods to disperse Pt clusters on CdS nanorod, Heiz et al. suggested that the optimal size of Pt nanoparticles is ∼1 nm for photocatalytic HER.[7] Similarly, the ∼1 nm size is also identified as the optimal size for CO_2 photoreduction on TiO_2 support.[8] In contrast to nanosized Pt particles, Yang et al., with chemical etching, generated very

Received: May 16, 2018
Revised: June 13, 2018
Published: June 22, 2018

DOI: 10.1021/acscatal.8b01886
ACS Catal. 2018, 8, 7270−7278

small Pt clusters (contain a few atoms, being invisible under transmission electron microscopy (TEM)) on anatase TiO_2 and found that they are active sites for photocatalytic hydrogen production as evidenced from extended X-ray absorption fine structure (EXAFS) spectra.[9] Despite there being no general consensus achieved on the optimum particle size, these experiments do suggest that HER prefers to occur on small metallic particles, neither bulky metal nor isolated metallic ions, implying multiple metal atoms on the surface are necessary for H_2 evolution and the size of metal particles matters in the rate-determining step of HER.

Because of the added complexity of photocatalytic reactions, current views are divided on the origin of the high activity of (sub)nano metal particles. On the one hand, since Pt is also the common catalyst for HER under electrochemical conditions, it was naturally expected that the low-coordinated sites (e.g., apex sites) on small Pt particles that has high activity for Tafel reaction (H−H coupling on surface)[9−11] are responsible for the activity increase. On the other hand, the charge separation during photocatalytic reaction may also benefit from the supported metal particles. Bahnemann and Kamat have studied the charge transfer efficiency from oxide to metal using time-resolved transient absorption spectra (TAS), and they show that surface-deposited small metal particles, such as Pt and Au, act as efficient electron scavengers competing with the undesired recombination.[12,13] Also using the TAS technique, Patrocinio[14] and Biswas[8] reported the efficient electron−hole separation induced by Pt nanoparticles and suggested that the subsequent electron transfer might be the key factor for the enhanced photoactivity. It was also noticed that the electron transfer was sensitive to the electronic structures of metal clusters:[7,13] small particles of ∼1 nm size could pin a desirable Fermi level to accept photoelectrons from oxide as found by Heiz et al.;[7] instead, large Pt particles could also consume photoholes, thus serving as recombination centers and leading to decreased photoactivity.[15]

In fact, the deposition of metal particles on oxides often causes charge redistribution at the interface, leading to a strong metal−support interaction (SMSI),[16] which would consequently affect the catalytic properties of deposited metals.[17−19] Umezawa et al. investigated electronic structures for metal/TiO_2 interface (metal = Pt, Pd, Au), with density functional theory (DFT) calculations, and demonstrated that the charge redistribution occurs largely locally: the effect drops quickly from the first contact metal layer to the second and to the third layer; beyond the third layer, the charge depletion/accumulation becomes negligible.[20] Similar phenomena have also been observed at other metal/oxide interfaces.[21,22] It implies that the first three metal layers on oxide may exhibit distinct catalytic behaviors compared to bulk metals.

In this work, we aim to rationalize the size effect of supported Pt particles on TiO_2 in the photocatalytic HER by evaluating the energetics of surface catalysis and the electron transfer in a unified theoretical framework. The model system of anatase TiO_2 (101) supported Pt clusters is selected, where four different structures, namely, Pt_5/TiO_2, Pt_8/TiO_2, Pt_{13}/TiO_2, and Pt_{19}/TiO_2 representing one-, quasi two-, two-, and three-Pt-layer geometries, respectively, are constructed and simulated using extensive ab initio molecular dynamics (AIMD). We demonstrate that the electronic properties of supported metals are very sensitive to the particle size, and for photocatalytic HER, the surface catalytic activity and electron-transfer efficiency follow different size-dependent trends. Consequently, one must balance these aspects to maximize the photoactivity.

2. DFT CALCULATION DETAILS AND MODELS

DFT Calculations. All DFT calculations were performed using the VASP program[23,24] with the spin-polarization being considered. The DFT functional was utilized at the Perdew−Burke−Ernzerhof (PBE) level. The project-augmented wave (PAW) method was used to represent the core−valence electron interaction. The valence electronic states were expanded in plane-wave basis sets with energy cutoff at 450 eV. The ionic degrees of freedom were relaxed using the conjugate gradient and quasi-Newton Broyden minimization scheme, until the Hellman−Feynman forces on each ion were less than 0.05 eV/Å. The transition states were searched using a constrained optimization scheme[25,26] and were verified when (i) all forces on atoms vanish and (ii) the total energy is a maximum along the reaction coordination but a minimum with respect to the rest of the degrees of freedom. The force threshold for the transition state (TS) search was 0.05 eV/Å. The dipole correction was applied throughout the calculations to take the polarization effect into account.[26,27] To speed up the AIMD simulation, a $(1 \times 1 \times 1)$ k-points mesh was used for all structural dynamics, and a $(2 \times 2 \times 1)$ mesh was utilized for converging the energetics.

For TiO_2 system, we demonstrated previously[28,29] that the DFT+U method[30] can yield similar structures and energies as those from the hybrid DFT (HSE06 functional) method. Here we mainly applied the DFT+U method in computing the thermodynamic properties (e.g., adsorption energy, thermal stability, etc.), where the on-site coulomb correction was set on Ti 3d orbitals with an effective U value of 4.2 eV as suggested in other theoretical works.[30,31] To produce the electronic structure properties more accurately[32] (e.g., band gap, band edge position, charge distribution, etc.), we further performed hybrid HSE06 calculations with the DFT+U geometry. In HSE06 calculation, the electronic minimization algorithm utilized was the Damped method with a very soft augmentation charge (PRECFOCK = Fast). The HSE06 optimized lattice and the band gap for the bulk anatase TiO_2 ($a = b = 3.766$, $c = 9.448$ Å; $E_g = 3.31$ eV; see Figure S1 in the Supporting Information) agree well with the experimental data ($a = b = 3.776$, $c = 9.486$ Å; $E_g \approx 3.2$ eV).

The adsorption energy of hydrogen atom (E_{ad}^{H}) is defined as the energy difference before and after the adsorption with respect to the gas-phase H_2 molecule as shown below:

$$E_{ad}^{H} = E(\text{total}) - E(\text{surface}) - 0.5E(H_2)$$

where E(surface), $E(H_2)$, and E(total) are the energies for the clean surface, H_2 molecule in the gas phase, and hydrogen atom adsorbed on the surface, respectively. The Gibbs free energy of H adsorption (ΔG_H) is obtained by applying the entropy correction proposed by Norskov et al., that is, $\Delta G_H = E_{ad}^{H} + 0.24$.[33,34] The more negative the E_{ad}^{H} (or ΔG_H) is, the more strongly the H atom binds on surface.

Model for Pt/TiO_2 Composites. To accommodate Pt clusters, we utilized a relatively large supercell of anatase (101) surface, namely, a $p(2 \times 3)$ periodic slab with three TiO_2 layers (72 Ti and 36 O atoms) and a vacuum of 16 Å between slabs. We checked our key results, for example, the energetics of electron transfer, by enlarging the slab model to four layers, which produces similar results as that from three-layer

DOI: 10.1021/acscatal.8b01886
ACS Catal. 2018, 8, 7270−7278

calculations (see Table S1 in the Supporting Information), consistent with previous works.[35,36]

The extra photoelectron in systems was simulated by adding an excess electron into the supercell as common practice.[31,36,37] We also checked the approach by comparing the electron transfer results with that obtained by introducing an additional H atom on the opposite layer of TiO_2 slab in charge-neutral systems (see results in Table S1). The localization of electron on a particular Ti site of TiO_2 can be initially configured and followed by DFT+U electronic structure optimization. Initial magnetic moments on each atom are usually necessary in the input setting, although they will be optimized during the calculation. Site-projected magnetic moments and the Bader charge analyses are calculated to ensure the localization of the electron, while the spin density is visualized by the isodensity surface.

In computing the electron-transfer energies, we utilized four types of $Pt/TiO_2(101)$ systems with different electronic configurations, which can be verified by inspecting their electron density distribution:

(i) Pt/TiO_2 after H adsorption that is overall charge neural.
(ii) Pt/TiO_2 with one proton on Pt and one electron localized in bulk TiO_2 that is overall charge neutral but with spatially separated charge.
(iii) Pt/TiO_2 with one extra electron delocalized on the Pt cluster that is negatively charged.
(iv) Pt/TiO_2 with one extra electron localized in bulk TiO_2 that is negatively charged.

For the charged systems (iii) and (iv), a compensating uniform background countercharge is introduced systematically to recover the neutrality of lattice. By computing the energetics of the four models, we can readily evaluate the electron-transfer energetics following the *proton-promoted electron-transfer* mechanism, $\Delta E(\mathrm{PPET}) = E_{(\mathrm{i})} - E_{(\mathrm{ii})}$ and following the *intrinsic electron-transfer* mechanism, $\Delta E(\mathrm{IET}) = E_{(\mathrm{iii})} - E_{(\mathrm{iv})}$, where $E_{(\mathrm{x})}$ is the DFT energy of the corresponding (x) model.

To determine the structures of Pt/TiO_2 composites, AIMD simulation was performed to search for the optimal structures (the most stable structure obtained from our AIMD trajectories) of Pt clusters on TiO_2 slab. The simulation was performed in the canonical (NVT) ensemble employing Nosé–Hoover thermostats. The temperature was set at 450 K that is taken from the temperature of hydrothermal treatment commonly used in experiments,[6,38] and the time step was 1 fs. More than 20 ps AIMD simulation was performed, and all the simulations reach the equilibrium plateau after ~8 ps (Figure S2). From the equilibrated trajectory (>8 ps), we select structural configurations in every 1 ps interval and fully optimize them until all forces diminish. From in total 14 structural candidates (see Table S2 in the Supporting Information), we determine the optimal (lowest energy) Pt/TiO_2 structures.

3. RESULTS AND DISCUSSION

3.1. Geometry Structures of Pt/TiO_2 Composites. Our investigation starts by searching for the physically sound metal/oxide interface model (Figure 1a–d) using long-time AIMD simulation (>20 ps, at 450 K; see methods). Taking the $Pt_{13}/TiO_2(101)$ system as an example, our AIMD simulation is briefly described as follows. The Pt_{13} initial structure is taken from the well-known icosahedral Pt_{13} cluster that is a high-symmetry stable minimum in the gas phase.[39] The AIMD simulation is then performed, and all the structures along the trajectory are recorded (Figure 1e). We found that the supported Pt_{13} cluster undergoes restructuring rapidly in the first 2 ps and reaches the equilibrium plateau after ~8 ps. The

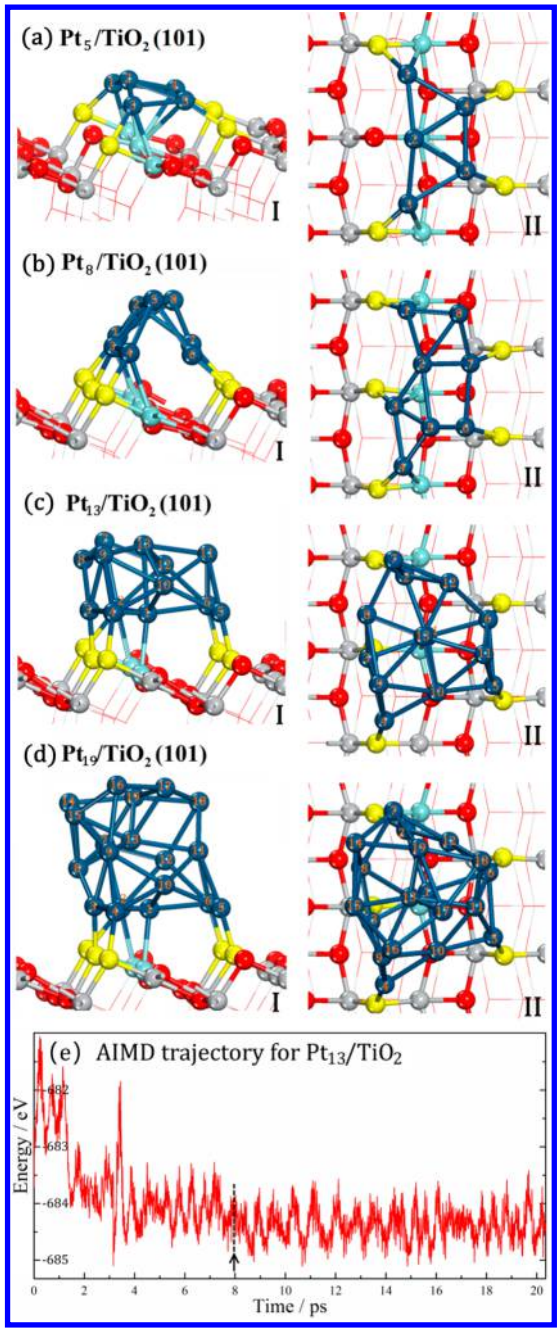

Figure 1. Geometry structures for (a) one-Pt-layer model of $Pt_5/TiO_2(101)$, (b) quasi two-Pt-layer model of $Pt_8/TiO_2(101)$, (c) two-Pt-layer model of $Pt_{13}/TiO_2(101)$, and (d) three-Pt-layer model of $Pt_{19}/TiO_2(101)$ composites, respectively. Both the side view (I) and top view (II) are illustrated, and all Pt atoms are indexed with Arabic numbers. (e) AIMD trajectory for the Pt_{13}/TiO_2 composite. Others are provided in Figure S2 in the Supporting Information. The equilibration in AIMD occurs after ~8 ps as indicated by the black arrow. The O and Ti anchoring sites in contact with Pt cluster are highlighted in yellow and light blue colors, respectively. Gray: Ti; red: O; dark cyan: Pt; white: H. This color scheme is used throughout the paper.

DOI: 10.1021/acscatal.8b01886
ACS Catal. 2018, 8, 7270–7278

structures with relatively low potential energy with ~1 ps interval along the equilibrated molecular dynamics (MD) trajectory (>8 ps) are then selected and fully relaxed in geometry. The optimal $Pt_{13}/TiO_2(101)$ structure is finally determined from these structural candidates (see calculation details in Section 2), which are highlighted in Figure 1c (with both side and top views). Similarly, the optimal structures for Pt_8/TiO_2 and Pt_{19}/TiO_2 are also determined from AIMD simulations, as shown in Figure 1b,d, where their initial structures were built by removing the outermost layer of the optimal Pt_{13}/TiO_2 structure for the Pt_8/TiO_2 model, while adding a third layer ($Pt^{\#14}$–$Pt^{\#19}$) for the Pt_{19}/TiO_2, respectively. Their MD trajectories (>20 ps) are provided in Figure S2.

From Figure 1b–d, we notice that the Pt_8 and Pt_{13} clusters prefer two-layer geometries and that Pt_{19} has a three-layer morphology, suggesting the larger Pt–Pt interaction compared to the Pt-oxide interaction, consistent with results of Musgrave et al.[40] To better understand the properties of the one-layer Pt cluster, we also calculated a very small Pt_5 cluster for the purpose of comparison, that is, the $Pt_5/TiO_2(101)$, where only local geometry optimization is performed to determine the best geometry from several manually constructed one-layer candidates. The lowest-energy one-layer Pt_5/TiO_2 structure is also shown in Figure 1a. It should be mentioned that those Pt/TiO_2 structures in Figure 1 might not be the global minimum of Pt clusters on TiO_2, considering the great complexity of the potential energy surface[10] and the relatively short time in AIMD simulations. However, as we are concerned for the size and layer dependence of the catalytic activity in the Pt/TiO_2 system, they do represent Pt clusters with different layers that have relatively high stability. Results are summarized in Table 1.

Table 1. Summarized Properties of Four Pt/TiO_2 Composites, Including: Number of Pt Layers ($N_{Pt\text{-}layers}$), the Vertical Height of the Cluster (h), Number of Pt–O (N_{Pt-O}) and Pt–Ti Bonds (N_{Pt-Ti}), the Averaged Coordination of Pt Atom (N_{coord})[a]

					N_{coord}		
models	$N_{Pt\text{-}layers}$	h, Å	N_{Pt-O}	N_{Pt-Ti}	overall	top	ΔE/Pt
Pt_5/TiO_2	1	2.0	4	5	3	1	0.02
Pt_8/TiO_2	2	4.4	5	3	3	3	−0.35
Pt_{13}/TiO_2	2	5.2	5	2	5	3	−0.51
Pt_{19}/TiO_2	3	7.5	5	2	5	3	−0.63

[a]Both the overall N_{coord} and that in the top Pt layer are computed. The thermodynamic stability per Pt atom (ΔE/Pt), relative to that in the gaseous Pt_{13} icosahedron, is also listed (unit: eV).

The $Pt_5/TiO_2(101)$ has a flat one-Pt-layer architecture as shown in Figure 1a (**one-Pt-layer model**). Four Pt–O and five Pt–Ti bonds are involved to bind the Pt_5 cluster on TiO_2 surface with a vertical height of ~2.0 Å. The averaged coordination number (N_{coord}) of Pt is extremely low, being ~3 for the overall N_{coord} and ~1 for that in the top Pt layer (only Pt–Pt bonds are included). Even in such structure, the thermodynamic stability of Pt atom is generally comparable to that in the gaseous Pt_{13} icosahedron (Table 1).

For the optimal structure of $Pt_8/TiO_2(101)$ in Figure 1b, the Pt_8 cluster has a rooflike architecture with a ridge composed of three Pt atoms ($Pt^{\#2}$, $Pt^{\#5}$, $Pt^{\#8}$). The bottom two rows anchor to the surface through five Pt–O and three Pt–Ti bonds. The overall vertical height is ~4.4 Å, being slightly lower by ~0.8 Å than the two-Pt-layer model. The cluster is more like a transition structure between one-layer and two-layer Pt clusters (**quasi two-Pt-layer model**), with its bottom two rows approaching to each other although still being separated by ~3.3 Å (Pt–Pt bond: ~2.6 Å). Apparently, the amorphous structure of Pt_8 cluster is due to the very low N_{coord} of ~3: a folded rooflike architecture can increase the atomic proximity and stabilize the interface structure, as confirmed by the thermostability (Table 1).

The optimal $Pt_{13}/TiO_2(101)$ in Figure 1c features with a largely distorted low-symmetry Pt_{13} cluster with roughly a two-layer architecture (**two-Pt-layer model**). In this structure, six Pt atoms ($Pt^{\#1}$–$Pt^{\#6}$) in the bottom layer are involved to bond with the TiO_2 surface via five Pt–O bonds and two Pt–Ti bonds. The other seven Pt atoms ($Pt^{\#7}$–$Pt^{\#13}$) constitute the upper layer, where most Pt atoms are at the apex site with only approximately three coordinations. In contrast to the initial Pt_{13} icosahedron, the area covered by Pt_{13} on the surface increases by ~30%, while the vertical height (5.2 Å) shrinks 19%, apparently owing to the flattening of the cluster on TiO_2 surface.[17] Accordingly, there exists a large energy gain of −0.51 eV per Pt atom, as the icosahedron was deposited on TiO_2, evidencing the SMSI in the system.

For the optimal $Pt_{19}/TiO_2(101)$ in Figure 1d, the Pt_{19} cluster has three-layer architecture (**three-Pt-layer model**) with a vertical height of ~7.5 Å. The top layer exposes an open structure composed of a triangle ($Pt^{\#17}$-$Pt^{\#18}$-$Pt^{\#19}$) neighboring with a pentagon ($Pt^{\#14}$-$Pt^{\#15}$-$Pt^{\#16}$-$Pt^{\#17}$-$Pt^{\#19}$), and all these Pt atoms have quite low N_{coord} of ~3. Comparing with the Pt_{13}/TiO_2 composite, we note that the geometry of bottom two layers ($Pt^{\#1}$–$Pt^{\#13}$) are quite similar, including the anchoring bonds. The overall N_{coord} in Pt_{19} is ~5, which is also equal to that of deposited Pt_{13} cluster. In general, the geometric properties of the three-layer Pt_{19}/TiO_2 largely resembles that of the two-layer Pt_{13}/TiO_2.

3.2. Electronic Structures. To compare the photoelectron-transfer efficiency for different Pt/TiO_2 models, we analyzed the electronic structures of four Pt/TiO_2 composites. In Figure 2, we show the density of states (DOS) of the systems as computed from hybrid HSE06 functional. All the band alignment is made by referencing to the valence band maximum (VBM) of TiO_2. We find that, for all these Pt/TiO_2 composites, a small band gap of 0.5–1.3 eV is formed between the occupied $5d_{Pt}$ and the empty $3d_{Ti}$ states. For the TiO_2 support (DOS shown in yellow-green curves), loading of Pt clusters hardly causes significant changes to the band structure of the oxide. For the Pt clusters (DOS in the blue curves), the metallic Pt states (before deposition; see Figure S3 in the Supporting Information) open a band gap of 0.8–1.3 eV (depending on the cluster size) as they are deposited on TiO_2. These occupied Pt states largely fill the gap of TiO_2 and lift the Fermi level (E_f) to a position close to the conduction band minimum (CBM) of TiO_2. The unoccupied Pt states are generally higher than CBM of TiO_2 and have a low contribution to the overall DOS.

In Figure 2a,b, the Pt_5/TiO_2 and Pt_8/TiO_2 composites show frail Pt states with small intervals (<0.1 eV) below the E_f and very large band gaps of 1.28 and 0.87 eV, respectively, suggesting the strong interaction between the interfacial first Pt layer and TiO_2 support.[20] By depositing a second layer, the Pt_{13} cluster introduces a smooth DOS in the gap of TiO_2 and moves up the E_f position with a band gap of 0.45 eV (Figure

DOI: 10.1021/acscatal.8b01886
ACS Catal. 2018, 8, 7270–7278

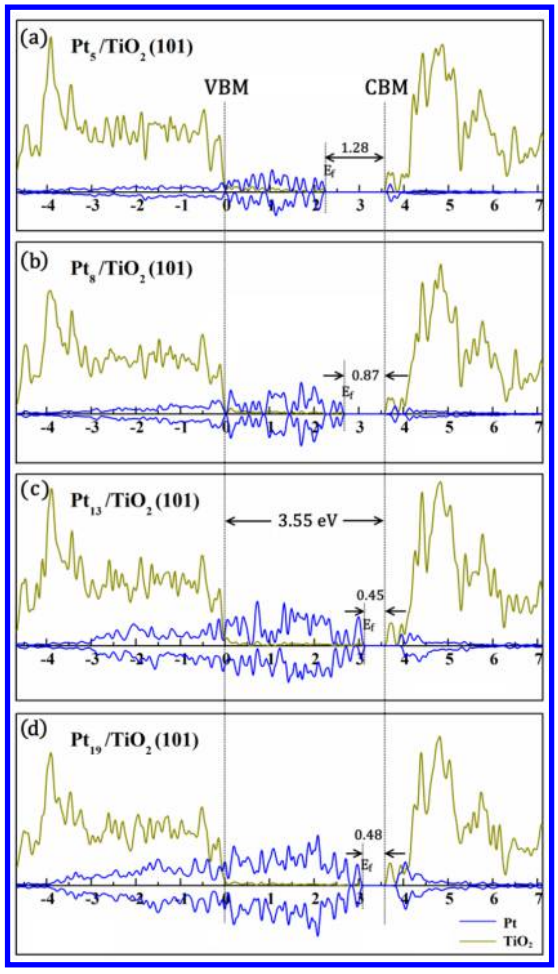

Figure 2. Computed DOS using hybrid HSE06 functional for (a) $Pt_5/TiO_2(101)$, (b) $Pt_8/TiO_2(101)$, (c) $Pt_{13}/TiO_2(101)$, and (d) $Pt_{19}/TiO_2(101)$ composites, respectively. The DOS for Pt clusters and for anatase surface are represented by blue and yellow-green curves, respectively. The vertical dot lines indicate the VBM and CBM of anatase $TiO_2(101)$, respectively. The band gap of $TiO_2(101)$ and the optimal Pt/TiO_2 composites are indicated by a pair of arrows.

2c). For the three-Pt-layer Pt_{19}/TiO_2 composite (Figure 2d), the Pt states becomes much richer and smoother, but the E_f locates close to that in the Pt_{13}/TiO_2, being 0.48 eV below the CBM. A clear layer-dependent trend for the electronic structure (band gap) has been identified: Pt_5/TiO_2 > Pt_8/TiO_2 > $Pt_{13}/TiO_2 \approx Pt_{19}/TiO_2$.

The observed trend for DOS is consistent with our Bader charge analyses, which show that all Pt clusters become positively charged after deposition on TiO_2 (Table S3 in the Supporting Information), consistent with previous works.[40,41] We found that each Pt atom in the Pt_5 cluster is positively charged by +0.13 |e| on average, showing the weakest metallic characters, while those in the Pt_{19} carry the smallest positive charge of +0.05 |e| per atom. In addition, the lifted E_f (relative to the VBM of TiO_2) enables Pt/TiO_2 to utilize the visible light as confirmed by the calculated light adsorption spectrum (see Figure S4), which explains the observed photocatalytic activities of Pt/TiO_2 under visible-light illumination.[6,42]

Our DOS results indicate that (i) the deposited Pt_5 is severely passivated by the oxide, showing the lowest E_f and largest band gap; (ii) Pt_{13} and Pt_{19} may have comparable bonding properties in surface reactions because of their similar electronic structures and also atomic coordinations (Table 1); (iii) the electronic properties of deposited Pt_8 are again in the transition between the one-Pt-layer and multi-Pt-layer clusters.

3.3. Electron Transfer. With the knowledge of the band structure, we are now at the position to address the electron-transfer efficiency in Pt/TiO_2 systems. It was shown that photogenerated electrons are first produced in the bulk region of TiO_2 after photon excitation[36,43,44] and become self-trapped on Ti cations to yield Ti^{3+} within a few picoseconds.[45,46] They are then transferred to the metal cocatalyst to promote the surface HER. In our previous work,[17] we demonstrated that first-principles calculations can be utilized to evaluate the energetics for the electron transfer from bulk TiO_2 to the metal. We found that a PPET mechanism is universally present in the metal/TiO_2 systems in photocatalytic HER, which can be energetically much more favorable compared to the IET without the presence of proton (Figure S5). Here, we continued to evaluate the PPET and IET energies on different Pt/TiO_2 systems.

Similar to our previous work,[17] the extra electron localized at the subsurface of TiO_2 slab is taken as the initial state. The spin density for this trapped electron is shown in Figure 3a–d,

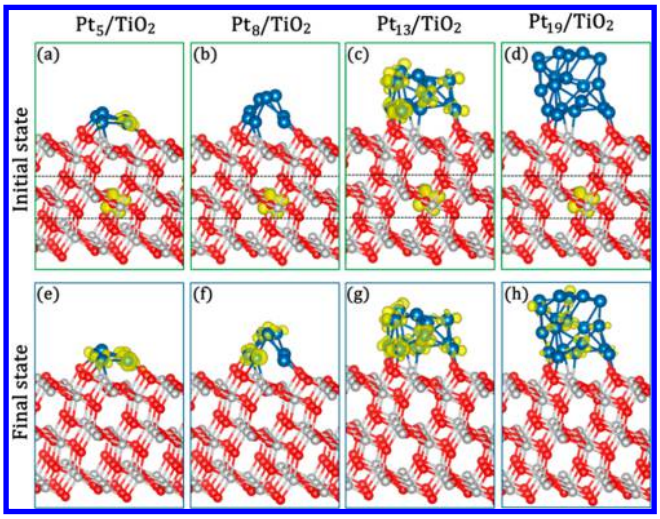

Figure 3. Spin-density plots (isovalue of 0.005 |e|/bohr^3) for both the initial state (a–d; green frames) and the final state (e–h; blue frames) during the electron transfer in Pt_5/TiO_2, Pt_8/TiO_2, Pt_{13}/TiO_2, and Pt_{19}/TiO_2 composites, respectively. The directional electron transfer from subsurface TiO_2 to Pt clusters is clearly illustrated.

featuring the characteristic d orbital shape. The final state is set as the extra electron onto Pt clusters as shown in Figure 3e–h, which becomes quite delocalized over all Pt atoms of the cluster as evidence from the spin-density plot. The energetics for the electron transfer with (PPET) and without (IET) the proton adsorption on the Pt clusters are then calculated, and the data are listed in Table 2. It should be mentioned that as there are many possible Ti atoms in the subsurface region of TiO_2 (indicated by dashed lines in Figure 3a–d) and also many possible proton adsorption sites on the surface of Pt clusters (site 1–4 in Table 2), we calculated different combinations of the electron trapping sites (Figures S6 and S7 in the Supporting Information) for each Pt/TiO_2 composites, and the reported energies are the averaged value.

From Table 2, we found that, in the clean Pt_5/TiO_2 and Pt_8/TiO_2 composites, the electron transfer from the TiO_2

DOI: 10.1021/acscatal.8b01886
ACS Catal. 2018, 8, 7270–7278

Table 2. Energetics for Two Ways of Electron Transfer (IET and PPET) from Bulk TiO_2 to Pt Clusters in Pt_5/TiO_2, Pt_8/TiO_2, Pt_{13}/TiO_2, and Pt_{19}/TiO_2 Composites, Respectively[a]

		PPET				
items models	IET clean surface	1	2	3	4	average
Pt_5/TiO_2	−0.39 (−0.34)	−0.61 (−0.47)	−0.50 (−0.39)	−0.52	−0.52	−0.54
Pt_8/TiO_2	−0.17 (−0.16)	−0.31 (−0.22)	−0.48 (−0.41)	−0.53	−0.27	−0.40
Pt_{13}/TiO_2[b]	0.05 (0.10)	−0.38 (−0.26)	−0.33 (−0.21)	−0.35	−0.27	−0.33
Pt_{19}/TiO_2	0.01 (0.04)	−0.30 (−0.20)	−0.32 (−0.18)	−0.28	−0.35	−0.31

[a]For the PPET mechanism, four different proton adsorption sites (1−4, corresponding to adsorption structures in Figures S9−S12 in the Supporting Information) are considered, and the averaged energies are listed for comparison. The influence of water environment on IET and PPET is also indicated by energies in parentheses. Energy unit: electronvolts. [b]Electron transfer energies (IET and PPET) for the Pt_{13}/TiO_2 composite is taken from ref 17.

subsurface to the Pt cluster releases energy of 0.39 and 0.17 eV respectively, suggesting a thermodynamically favored IET process. But it turns out to be endothermic for the clean Pt_{13}/TiO_2 and Pt_{19}/TiO_2 composites. This is consistent with the electronic structures (E_f position) in Figure 2, because a relatively lower energy level is beneficial to accept electrons.

For the PPET process, the directional electron transfer can be markedly boosted by surface adsorption of proton.[17] Regarding the Pt_5/TiO_2 and Pt_8/TiO_2 composites, we found that the electron transfer gets further promoted by −0.15 and −0.23 eV, respectively, via the PPET mechanism, but in general both the IET and PPET are fundamentally important. For the Pt_{13}/TiO_2 and Pt_{19}/TiO_2, the averaged PPET energy is −0.33 and −0.31 eV, respectively, being much more favored than the endothermic IET energies. Therefore, for TiO_2-supported metal (sub)nanoparticles composed of two or three metal layers, the PPET is the leading way of electron transfer in photocatalysis.

Obviously, the energy preference of the PPET should be related to the unique electronic structure of the proton-Pt/TiO_2 systems. By comparing the proton-Pt/TiO_2 system with the clean Pt/TiO_2 system, two key features from our results can be outlined. First, the Fermi level E_f (line III in Figure S5) is particularly down-shifted in the proton-Pt/TiO_2 system relative to the clean Pt/TiO_2 system. Second, the bottom of the unoccupied Pt states (line IV) is also much down-shifted and becomes close to or even lower than the CBM of TiO_2. All these changes caused by proton adsorption could facilitate the electron transfer from TiO_2 to Pt and subsequently help to accommodate the delocalized electron on Pt clusters.

Finally, we also investigated the influence of water environment, where both aqueous and adsorbed water molecules are considered, on the electron-transfer energies, as shown in Table 2. It was found that the existence of local water environment slightly retards the directional electron-transfer process by ∼0.04 eV for the IET process and ∼0.11 eV for the PPET, respectively. The larger impact on the PPET process is probably caused by the formation of hydrogen bond between surface-adsorbed proton and water molecules nearby (Figure S8 in the Supporting Information). Nevertheless, the general trend is well-reserved in all considered situations. Overall, we demonstrate that the electron-transfer efficiency follows the order of $Pt_5/TiO_2 > Pt_8/TiO_2 > Pt_{13}/TiO_2 \approx Pt_{19}/TiO_2$, and the electron transfer follows mainly the PPET mechanism.

3.4. Surface Catalysis. After the electron transfer to Pt clusters and formation of surface H atom ($H^+ + e^- \rightarrow H_{ads}$), HER can then occur following the Tafel mechanism, $H_{ads} + H_{ads} \rightarrow H_2$ (basically a surface reaction with zero net charge).[47,48] For HER on metals, the ΔG_H is generally taken as the activity descriptor, and catalytic sites with too strong or endothermic ΔG_H would present low activity.[33,34] For the Pt/TiO_2 composites, differing from the extended surface, there are many possible H adsorption sites on Pt clusters (Figure 1). By considering the ΔG_H−activity relation (volcano curve),[33,34] we first determined ΔG_H on each Pt site on all the Pt/TiO_2 composites (Figures S9−S12 and Table S4), and then selected two of the most reactive sites with ΔG_H approaches zero for computing the H−H coupling barrier (E_a^{coup}) and determining the activity trend.

In Figure 4, we show the calculated energetics and the transition states for H_2 coupling on these Pt clusters. From Figure 4a−d, one can see that surface adsorption of H atom on

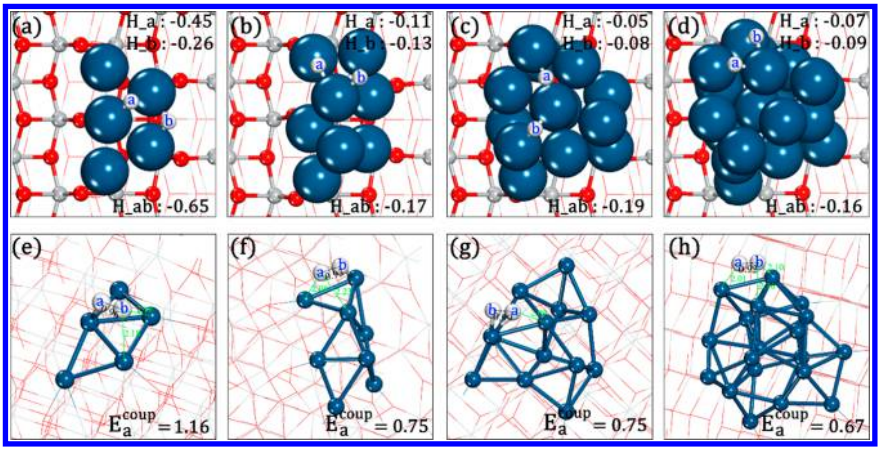

Figure 4. Geometry structures for (a−d) H adsorption at two reactive sites (site a and b) and (e−h) transition states of H−H coupling on Pt_5/TiO_2, Pt_8/TiO_2, Pt_{13}/TiO_2, and Pt_{19}/TiO_2 composites, respectively. Gibbs adsorption energies for the independent adsorption of H atom on each of the two reactive sites (H_a and H_b), the coadsorption of two H atoms (H_ab), as well as the H−H coupling barrier, are listed, respectively. Energy unit: electronvolts.

DOI: 10.1021/acscatal.8b01886
ACS Catal. 2018, 8, 7270−7278

Pt clusters favors the bridge site configuration. The independent adsorption of H atom on each of the two reactive sites (ΔG_{H_a} and ΔG_{H_b}) show large variations for the one-Pt-layer model Pt_5/TiO_2, while they are generally comparable among the other three models. The coadsorption strength of two H atoms (ΔG_{H_ab}) was found approximately the sum of two independent adsorptions on all of four Pt clusters. Obviously, all the three multi-Pt-layer Pt/TiO_2 composites (Figure 4b–d) show averaged ΔG_{H_ab} approaching the volcano peak (ΔG_H = 0 eV), manifesting themselves to be very good catalysts for catalyzing HER. But the activity of Pt_5/TiO_2 (Figure 4a) is expected to be much lower than the others, because the ΔG_{H_ab} is far from the peak position.

At the transition state, as shown in Figure 4e–h, at least one of the two H atoms must migrate from the bridge adsorption into an off-top configuration. The other H moves toward the off-top H with its Pt–H bonds stretched from ~1.8 to ~2.1 Å. The computed energy barrier E_a^{coup} is 1.16, 0.75, 0.75, and 0.67 eV for Pt_5/TiO_2, Pt_8/TiO_2, Pt_{13}/TiO_2, and Pt_{19}/TiO_2, respectively, consistent with their adsorption strength. Considering the E_a^{coup} of 0.88 and 1.07 eV on the surface of Pt(111) and Pt(100), respectively,[10] the HER activity on Pt nanoparticles is generally enhanced. More importantly, from the calculated energetics (ΔG_H and E_a^{coup}), we can conclude that the H–H coupling activity on Pt clusters follows the order of $Pt_5/TiO_2 < Pt_8/TiO_2 \approx Pt_{13}/TiO_2 \approx Pt_{19}/TiO_2$.

3.5. Discussion on Particle Size Dependence of Photoactivity. From the above results, we show that the electron-transfer efficiency follows the order $Pt_5/TiO_2 > Pt_8/TiO_2 > Pt_{13}/TiO_2 \approx Pt_{19}/TiO_2$, while the surface catalytic activity follows a different order $Pt_5/TiO_2 < Pt_8/TiO_2 \approx Pt_{13}/TiO_2 \approx Pt_{19}/TiO_2$. The one-layer Pt_5, two-layer Pt_{13}, and three-layer Pt_{19} are all partially specialized in one aspect, but they are weak in the other. Accordingly, the overall photoactivity is expected to be underutilized and largely restricted by the weak point. Only the quasi-two-layer Pt_8, with a transition structure between the one- and the two-Pt-layer, integrates the good electron-transfer character of one-layer clusters with the high catalytic activity of the two-layer. This interesting finding should not be limited to the Pt_8 cluster but rather related to the quasi-two-layer morphology. Indeed, we also constructed another quasi two-Pt-layer Pt_7/TiO_2 composite (determined by AIMD) and examined its electron-transfer energy and surface catalytic activity, as shown in Figure S13 in the Supporting Information. The superior activity of this quasi two-Pt-layer structure for photocatalytic H_2 production is also identified: the computed electron-transfer energy (−0.15 eV for the IET and −0.40 eV for the PPET) and the H–H coupling barrier (E_a^{coup} = 0.81 eV) are all similar to that of the Pt_8/TiO_2, reaching a good balance between the surface catalytic activity and electron-transfer efficiency. In conclusion, a quasi-two-layer structure with rooflike ridges in the second layer is theoretically predicted as the finest shape of Pt cocatalyst on TiO_2 for photocatalytic HER.

Our results also imply that the photocatalytic properties for supported multi-Pt-layer nanoparticles basically converge as early as two Pt layers. This is evident as the two-Pt-layer Pt_{13}/TiO_2 and three-Pt-layer Pt_{19}/TiO_2 always show quite similar results in both the surface catalysis and the electron-transfer process. By further investigating a four-Pt-layer Pt_{25}/TiO_2 model (determined by AIMD) using the same calculation approach (see results in Figure S14 in the Supporting Information), we confirm the converged photocatalytic properties for multi-Pt-layer nanoparticles (at least two atomic layers), in agreement with the results of Chen et al. on charge redistribution at the metal/TiO_2 interface.[20]

In reality, the deposited Pt particles may have a wide range of size distribution, not limited to the Pt_5, Pt_7, Pt_8, Pt_{13}, Pt_{19}, and Pt_{25} investigated in this work. We propose to use a simplified model of a supported metal particle in a spherical segment[49,50] to present a rough estimation on the optimal size of Pt cocatalyst on TiO_2 in experiments for photocatalytic HER. Two parameters of the radius of curvature R and contact angle α are essential to describe a supported particle, as shown in Figure 5a. For metal cocatalysts on TiO_2 that exhibit the SMSI, the contact angle α is usually no more than $\pi/2$, and consequently the d and h are correlated as $d = \frac{2h \sin \partial}{1 - \cos \partial}$, $0 \le \partial \le \frac{\pi}{2}$. This is, for instance, a small α of $\pi/3$ was reported for Rh particles on TiO_2,[49] while it was assumed to be $\pi/2$ for the Pt/TiO_2 interface,[51] which are also consistent with our AIMD simulation obtained optimal Pt/TiO_2 structures (Figure 5b,c). Using this equation and assuming a contact angle window of ($\pi/3$, $\pi/2$), we can estimate the particle size of the quasi-two-layer Pt clusters to be 0.70–1.52 nm: from 0.88 to 1.52 nm if estimating according to the Pt_8/TiO_2 model (h = 4.4 Å), or 0.70 to 1.21 nm if estimating according to the Pt_7/TiO_2 model (h = 3.5 Å; Figure S13). For smaller Pt particles less than ~0.7 nm (one-Pt-layer), the surface catalytic activity would be low because of the too strong ΔG_H and large E_a^{coup}, while for particles larger than ~1.8 nm (multi-Pt-layer; at least two atomic layers), the corresponding electron-transfer efficiency would be limited. Optimally, deposited Pt nanoparticle with ~1 nm diameter is predicted to be the most active size for photocatalytic HER.

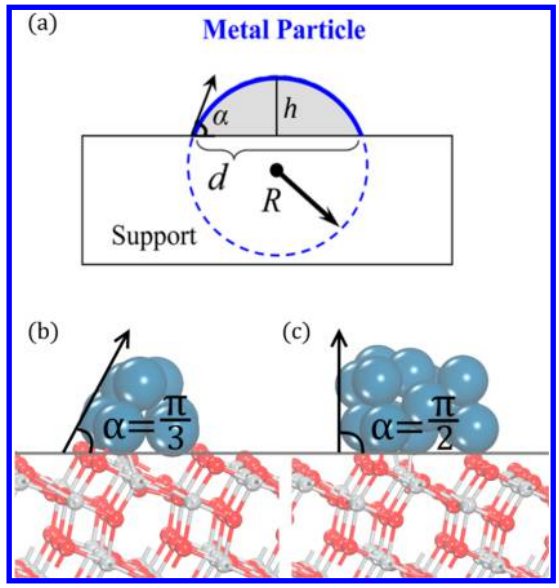

Figure 5. (a) Schematic of supported metal particle in a spherical segment with the radius of curvature R and the contact angle α between the particle and support. Two contact angles of (b) $\pi/3$ and (c) $\pi/2$ are evidenced from our AIMD obtained optimal Pt/TiO_2 structures. The diameter d and also the height h of the particle are also indicated.

DOI: 10.1021/acscatal.8b01886
ACS Catal. 2018, 8, 7270–7278

4. CONCLUSION

This work investigates the size effect of Pt cocatalyst on TiO_2 in photocatalytic HER, mainly concerning on the layer-dependent activity with two aspects of the surface catalysis and electron transfer included. Four Pt_n/TiO_2 composites (n = 5, 8, 13, 19) with one-, quasi two-, two-, and three-Pt-layer clusters were constructed explicitly. Our major conclusions are outlined as follows.

(i) Deposition of Pt clusters on TiO_2 splits the metallic Pt states and opens a gap of 0.5−1.3 eV depending on the cluster size. The electronic properties of supported Pt particles on TiO_2 are very sensitive to the particle size, which gradually turn to be less metallic as the number of Pt layers decreases.

(ii) The size-dependent activity of deposited Pt clusters follows different trend of $Pt_5/TiO_2 < Pt_8/TiO_2 \approx Pt_{13}/TiO_2 \approx Pt_{19}/TiO_2$ for the surface catalysis and $Pt_5/TiO_2 > Pt_8/TiO_2 > Pt_{13}/TiO_2 \approx Pt_{19}/TiO_2$ for the electron transfer. This indicates that the rate-determining step of photocatalytic HER on supported metal cocatalysts actually changes with the particle size.

(iii) The quasi two-Pt-layer structure with rooflike ridges in the second layer is theoretically identified as the finest shape of Pt cocatalyst on TiO_2 for photocatalytic HER, which approximately corresponds to an optimal particle size of 0.70−1.52 nm in experiments.

■ ASSOCIATED CONTENT

Supporting Information

The Supporting Information is available free of charge on the ACS Publications website at DOI: 10.1021/acscatal.8b01886.

The convergence test calculations on K-points mesh and TiO_2(101) slab layers; band structure of bulk anatase TiO_2; total energies of candidate structures and trajectories from AIMD simulations; computed DOS for Pt clusters in gas phase or on TiO_2 support with and/or without proton adsorption; simulated light-absorption spectrum for Pt/TiO_2 composites; spin-density plots for electron transfer via PPET mechanism; spin-density plots to illustrate possible electron-trapping sites at TiO_2 subsurface; influence of water surroundings on electron-transfer energies; surface H adsorption structures and also energies on four Pt/TiO_2 composites; summarized results on Pt_7/TiO_2 and Pt_{25}/TiO_2 composites; remarks on the "layer-dependent" and "size-dependent" (PDF)

■ AUTHOR INFORMATION

Corresponding Authors

*E-mail: zpliu@fudan.edu.cn. (Z.P.L.)

*E-mail: yangwm.sshy@sinopec.com. (W.M.Y.)

ORCID

Dong Wang: 0000-0001-5561-6425

Zhi-Pan Liu: 0000-0002-2906-5217

Notes

The authors declare no competing financial interest.

■ ACKNOWLEDGMENTS

The authors acknowledge the financial support from The National Key Research and Development Program of China (No. 2016YFB0701100, 2017YFB0702800), the National Natural Science Foundation of China (21533001), 973 Program (2013CB834603), Science and Technology Commission of Shanghai Municipality (08DZ2270500), and China Postdoctoral Science Foundation (2016M600348).

■ REFERENCES

(1) Chen, X.; Mao, S. S. Titanium Dioxide Nanomaterials: Synthesis, Properties, Modifications, and Applications. *Chem. Rev.* **2007**, *107*, 2891−2959.

(2) De Angelis, F.; Di Valentin, C.; Fantacci, S.; Vittadini, A.; Selloni, A. Theoretical Studies on Anatase and Less Common TiO_2 Phases: Bulk, Surfaces, and Nanomaterials. *Chem. Rev.* **2014**, *114*, 9708−9753.

(3) Thompson, T. L.; Yates, J. T., Jr Surface Science Studies of the Photoactivation of TiO_2-New Photochemical Processes. *Chem. Rev.* **2006**, *106*, 4428−4453.

(4) Yang, J.; Wang, D.; Han, H.; Li, C. Roles of Cocatalysts in Photocatalysis and Photoelectrocatalysis. *Acc. Chem. Res.* **2013**, *46*, 1900−1909.

(5) Ran, J.; Zhang, J.; Yu, J.; Jaroniec, M.; Qiao, S. Z. Earth-Abundant Cocatalysts for Semiconductor-Based Photocatalytic Water Splitting. *Chem. Soc. Rev.* **2014**, *43*, 7787−7812.

(6) Yu, J.; Qi, L.; Jaroniec, M. Hydrogen Production by Photocatalytic Water Splitting over Pt/TiO_2 Nanosheets with Exposed (001) Facets. *J. Phys. Chem. C* **2010**, *114*, 13118−13125.

(7) Schweinberger, F. F.; Berr, M. J.; Doblinger, M.; Wolff, C.; Sanwald, K. E.; Crampton, A. S.; Ridge, C. J.; Jackel, F.; Feldmann, J.; Tschurl, M.; Heiz, U. Cluster Size Effects in the Photocatalytic Hydrogen Evolution Reaction. *J. Am. Chem. Soc.* **2013**, *135*, 13262−13265.

(8) Wang, W.-N.; An, W.-J.; Ramalingam, B.; Mukherjee, S.; Niedzwiedzki, D. M.; Gangopadhyay, S.; Biswas, P. Size and Structure Matter: Enhanced CO_2 Photoreduction Efficiency by Size-Resolved Ultrafine Pt Nanoparticles on TiO_2 Single Crystals. *J. Am. Chem. Soc.* **2012**, *134*, 11276−11281.

(9) Xing, J.; Jiang, H. B.; Chen, J. F.; Li, Y. H.; Wu, L.; Yang, S.; Zheng, L. R.; Wang, H. F.; Hu, P.; Zhao, H. J.; Yang, H. G. Active Sites on Hydrogen Evolution Photocatalyst. *J. Mater. Chem. A* **2013**, *1*, 15258.

(10) Wei, G.-F.; Liu, Z.-P. Restructuring and Hydrogen Evolution on Pt Nanoparticle. *Chem. Sci.* **2015**, *6*, 1485−1490.

(11) Li, Y. H.; Peng, C.; Yang, S.; Wang, H. F.; Yang, H. G. Critical Roles of Co-catalysts for Molecular Hydrogen Formation in Photocatalysis. *J. Catal.* **2015**, *330*, 120−128.

(12) Bahnemann, D. W.; Hilgendorff, M.; Memming, R. Charge Carrier Dynamics at TiO_2 Particles: Reactivity of Free and Trapped Holes. *J. Phys. Chem. B* **1997**, *101*, 4265−4275.

(13) Subramanian, V.; Wolf, E. E.; Kamat, P. V. Catalysis with TiO_2/gold Nanocomposites. Effect of Metal Particle Size on the Fermi Level Equilibration. *J. Am. Chem. Soc.* **2004**, *126*, 4943−4950.

(14) Patrocinio, A. O. T.; Schneider, J.; França, M. D.; Santos, L. M.; Caixeta, B. P.; Machado, A. E. H.; Bahnemann, D. W. Charge Carrier Dynamics and Photocatalytic Behavior of TiO_2 Nanopowders Submitted to Hydrothermal or Conventional Heat Treatment. *RSC Adv.* **2015**, *5*, 70536−70545.

(15) Sadeghi, M.; Liu, W.; Zhang, T. G.; Stavropoulos, P.; Levy, B. Role of Photoinduced Charge Carrier Separation Distance in Heterogeneous Photocatalysis: Oxidative Degradation of CH_3OH Vapor in Contact with Pt/TiO_2 and Cofumed TiO_2−Fe_2O_3. *J. Phys. Chem.* **1996**, *100*, 19466−19474.

(16) Tauster, S. Strong Metal-Support Interactions. *Acc. Chem. Res.* **1987**, *20*, 389.

(17) Wang, D.; Liu, Z.-P.; Yang, W. Proton Promoted Electron Transfer in Photocatalysis: Key Step for Photocatalytic Hydrogen Evolution on Metal/Titania Composites. *ACS Catal.* **2017**, *7*, 2744−2752.

(18) Klyushin, A. Y.; Greiner, M. T.; Huang, X.; Lunkenbein, T.; Li, X.; Timpe, O.; Friedrich, M.; Hävecker, M.; Knop-Gericke, A.;

DOI: 10.1021/acscatal.8b01886
ACS Catal. 2018, 8, 7270−7278

Schlögl, R. Is Nanostructuring Sufficient to Get Catalytically Active Au? *ACS Catal.* **2016**, *6*, 3372−3380.
(19) Wang, Y. G.; Yoon, Y.; Glezakou, V. A.; Li, J.; Rousseau, R. The Role of Reducible Oxide-Metal Cluster Charge Transfer in Catalytic Processes: New Insights on the Catalytic Mechanism of CO Oxidation on Au/TiO_2 from Ab Initio Molecular Dynamics. *J. Am. Chem. Soc.* **2013**, *135*, 10673−10683.
(20) Chen, H.; Li, P.; Umezawa, N.; Abe, H.; Ye, J.; Shiraishi, K.; Ohta, A.; Miyazaki, S. Bonding and Electron Energy-Level Alignment at Metal/TiO_2 Interfaces: A Density Functional Theory Study. *J. Phys. Chem. C* **2016**, *120*, 5549−5556.
(21) Goniakowski, J. Electronic Structure of MgO-Supported Palladium Films: Influence of the Adsorption Site. *Phys. Rev. B: Condens. Matter Mater. Phys.* **1998**, *57*, 1935−1941.
(22) Bogicevic, A.; Jennison, D. R. Variations in the Nature of Metal Adsorption on Ultrathin Al_2O_3 Films. *Phys. Rev. Lett.* **1999**, *82*, 4050−4053.
(23) Kresse, G.; Furthmüller, J. Efficiency of Ab-Initio Total Energy Calculations for Metals and Semiconductors Using a Plane-Wave Basis Set. *Comput. Mater. Sci.* **1996**, *6*, 15−50.
(24) Kresse, G.; Hafner, J. Ab Initio Molecular-dynamics Simulation of the Liquid-Metal−Amorphous-Semiconductor Transition in Germanium. *Phys. Rev. B: Condens. Matter Mater. Phys.* **1994**, *49*, 14251−14269.
(25) Alavi, A.; Hu, P.; Deutsch, T.; Silvestrelli, P. L.; Hutter, J. CO Oxidation on Pt(111): An Ab Initio Density Functional Theory Study. *Phys. Rev. Lett.* **1998**, *80*, 3650−3653.
(26) Wang, D.; Jiang, J.; Wang, H.-F.; Hu, P. Revealing the Volcano-Shaped Activity Trend of Triiodide Reduction Reaction: A DFT Study Coupled with Microkinetic Analysis. *ACS Catal.* **2016**, *6*, 733−741.
(27) Hou, Y.; Wang, D.; Yang, X. H.; Fang, W. Q.; Zhang, B.; Wang, H. F.; Lu, G. Z.; Hu, P.; Zhao, H. J.; Yang, H. G. Rational Screening Low-Cost Counter Electrodes for Dye-Sensitized Solar Cells. *Nat. Commun.* **2013**, *4*, 1583.
(28) Wang, D.; Wang, H.-F.; Hu, P. Identifying the Distinct Features of Geometric Structures for Hole Trapping to Generate Radicals on Rutile TiO_2(110) in Photooxidation Using Density Functional Theory Calculations with Hybrid Functional. *Phys. Chem. Chem. Phys.* **2015**, *17*, 1549−1555.
(29) Wang, D.; Sheng, T.; Chen, J.; Wang, H.-F.; Hu, P. Identifying the Key Obstacle in Photocatalytic Oxygen Evolution on Rutile TiO_2. *Nat. Catal.* **2018**, *1*, 291−299.
(30) Morgan, B. J.; Watson, G. W. A DFT+U Description of Oxygen Vacancies at the TiO_2 Rutile (110) Surface. *Surf. Sci.* **2007**, *601*, 5034−5041.
(31) Yan, L. K.; Chen, H. N. Migration of Holstein Polarons in Anatase TiO_2. *J. Chem. Theory Comput.* **2014**, *10*, 4995−5001.
(32) Cheng, J.; Sulpizi, M.; VandeVondele, J.; Sprik, M. Hole Localization and Thermochemistry of Oxidative Dehydrogenation of Aqueous Rutile TiO_2(110). *ChemCatChem* **2012**, *4*, 636−640.
(33) Nørskov, J. K.; Bligaard, T.; Logadottir, A.; Kitchin, J. R.; Chen, J. G.; Pandelov, S.; Stimming, U. Trends in the Exchange Current for Hydrogen Evolution. *J. Electrochem. Soc.* **2005**, *152*, J23.
(34) Greeley, J.; Jaramillo, T. F.; Bonde, J.; Chorkendorff, I. B.; Norskov, J. K. Computational High-Throughput Screening of Electrocatalytic Materials for Hydrogen Evolution. *Nat. Mater.* **2006**, *5*, 909−913.
(35) Li, Y. F.; Selloni, A. Theoretical Study of Interfacial Electron Transfer from Reduced Anatase TiO_2(101) to Adsorbed O_2. *J. Am. Chem. Soc.* **2013**, *135*, 9195−9199.
(36) Di Valentin, C.; Selloni, A. Bulk and Surface Polarons in Photoexcited Anatase TiO_2. *J. Phys. Chem. Lett.* **2011**, *2*, 2223−2228.
(37) Ma, X.; Dai, Y.; Guo, M.; Huang, B. Relative Photooxidation and Photoreduction Activities of the {100}, {101}, and {001} Surfaces of Anatase TiO_2. *Langmuir* **2013**, *29*, 13647−13654.
(38) Ide, Y.; Inami, N.; Hattori, H.; Saito, K.; Sohmiya, M.; Tsunoji, N.; Komaguchi, K.; Sano, T.; Bando, Y.; Golberg, D.; Sugahara, Y. Remarkable Charge Separation and Photocatalytic Efficiency Enhancement through Interconnection of TiO_2 Nanoparticles by Hydrothermal Treatment. *Angew. Chem., Int. Ed.* **2016**, *55*, 3600−3605.
(39) Shichibu, Y.; Suzuki, K.; Konishi, K. Facile Synthesis and Optical Properties of Magic-Number Au_{13} Clusters. *Nanoscale* **2012**, *4*, 4125−4129.
(40) Muhich, C. L.; Zhou, Y.; Holder, A. M.; Weimer, A. W.; Musgrave, C. B. Effect of Surface Deposited Pt on the Photoactivity of TiO_2. *J. Phys. Chem. C* **2012**, *116*, 10138−10149.
(41) Jiang, D.-e.; Overbury, S. H.; Dai, S. Structures and Energetics of Pt Clusters on TiO_2: Interplay Between Metal−Metal Bonds and Metal−Oxygen Bonds. *J. Phys. Chem. C* **2012**, *116*, 21880−21885.
(42) Zhang, Z.; Wang, Z.; Cao, S.-W.; Xue, C. Au/Pt Nanoparticle-Decorated TiO_2 Nanofibers with Plasmon-Enhanced Photocatalytic Activities for Solar-to-Fuel Conversion. *J. Phys. Chem. C* **2013**, *117*, 25939−25947.
(43) Zhang, Z.; Yates, J. T. Direct Observation of Surface-Mediated Electron-Hole Pair Recombination in TiO_2(110). *J. Phys. Chem. C* **2010**, *114*, 3098−3101.
(44) Thompson, T. L.; Yates, J. T. Monitoring Hole Trapping in Photoexcited TiO_2(110) Using a Surface Photoreaction. *J. Phys. Chem. B* **2005**, *109*, 18230−18236.
(45) Tamaki, Y.; Furube, A.; Murai, M.; Hara, K.; Katoh, R.; Tachiya, M. Dynamics of Efficient Electron-hole Separation in TiO_2 Nanoparticles Revealed by Femtosecond Transient Absorption Spectroscopy Under the Weak-Excitation Condition. *Phys. Chem. Chem. Phys.* **2007**, *9*, 1453−1460.
(46) Tan, S.; Feng, H.; Ji, Y.; Wang, Y.; Zhao, J.; Zhao, A.; Wang, B.; Luo, Y.; Yang, J.; Hou, J. G. Observation of Photocatalytic Dissociation of Water on Terminal Ti Sites of TiO_2(110)-1 × 1 Surface. *J. Am. Chem. Soc.* **2012**, *134*, 9978−9985.
(47) Zou, X.; Zhang, Y. Noble Metal-free Hydrogen Evolution Catalysts for Water Splitting. *Chem. Soc. Rev.* **2015**, *44*, 5148−5180.
(48) Shi, Y.; Zhang, B. Recent Advances in Transition Metal Phosphide Nanomaterials: Synthesis and Applications in Hydrogen Evolution Reaction. *Chem. Soc. Rev.* **2016**, *45*, 1529−1541.
(49) Ouyang, R.; Liu, J.-X.; Li, W.-X. Atomistic Theory of Ostwald Ripening and Disintegration of Supported Metal Particles under Reaction Conditions. *J. Am. Chem. Soc.* **2013**, *135*, 1760−1771.
(50) Liu, J. C.; Wang, Y. G.; Li, J. Toward Rational Design of Oxide-Supported Single-Atom Catalysts: Atomic Dispersion of Gold on Ceria. *J. Am. Chem. Soc.* **2017**, *139*, 6190−6199.
(51) Schierbaum, K. D.; Fischer, S.; Torquemada, M. C.; de Segovia, J. L.; Román, E.; Martín-Gago, J. A. The Interaction of Pt with TiO_2(110) Surfaces: a Comparative XPS, UPS, ISS, and ESD Study. *Surf. Sci.* **1996**, *345*, 261−273.

DOI: 10.1021/acscatal.8b01886
ACS Catal. 2018, 8, 7270−7278